Design of a Haptic Arm Exoskeleton for Training and Rehabilitation

Abhishek Gupta, *Student Member, IEEE*, and Marcia K. O'Malley, *Member, IEEE*

***Abstract*—A high-quality haptic interface is typically characterized by low apparent inertia and damping, high structural stiffness, minimal backlash, and absence of mechanical singularities in the workspace. In addition to these specifications, exoskeleton haptic interface design involves consideration of space and weight limitations, workspace requirements, and the kinematic constraints placed on the device by the human arm. These constraints impose conflicting design requirements on the engineer attempting to design an arm exoskeleton. In this paper, the authors present a detailed review of the requirements and constraints that are involved in the design of a high-quality haptic arm exoskeleton. In this context, the design of a five-degree-of-freedom haptic arm exoskeleton for training and rehabilitation in virtual environments is presented. The device is capable of providing kinesthetic feedback to the joints of the lower arm and wrist of the operator, and will be used in future work for robot-assisted rehabilitation and training. Motivation for such applications is based on findings that show robot-assisted physical therapy aids in the rehabilitation process following neurological injuries. As a training tool, the device provides a means to implement flexible, repeatable, and safe training methodologies.**

***Index Terms*—Arm exoskeleton, design methodology, force feedback, haptic interface, robot aided rehabilitation.**

I. Introduction and Motivation

HAPTIC or force-reflecting interfaces are robotic devices used to display touch- or force-related sensory information from a virtual or remote environment to the user (see, for example, surveys [1]–[3]). Based on the point of attachment of the base of the robotic interface, haptic display devices can be classified as grounded [4] or ungrounded [5]. A grounded haptic device is affixed to a rigid base, transferring reaction forces to ground. An ungrounded haptic device is attached only to the operator's body, exerting reaction forces on the user at the point(s) of attachment. Typically, ungrounded haptic interfaces are good at providing feedback such as grasping forces during object manipulation. Alternatively, grounded devices perform better when displaying kinesthetic forces to the user, like forces that arise when simulating static surfaces [1]. The workspace of a grounded device is limited by the manipulator's link lengths and joint limits. Often, in the case of common desktop interfaces like the PHANToM Desktop by Sensable Technologies (workspace: 6.4-in wide $\times$ 4.8-in high $\times$ 4.8-in deep) or the Impulse Engine 2000 by Immersion Corporation (workspace: 6 in $\times$ 6 in), the workspace is limited when compared to that of the human arm as determined from the joint ranges of motion for the shoulder, elbow, and wrist. An ungrounded or wearable interface, in comparison, permits greater human movement during haptic interactions. However, the increased workspace for an ungrounded device is achieved at the expense of design simplicity.

The ability to interact mechanically with virtual objects through incorporation of haptic feedback allows users to manipulate objects in the simulated or remote environment with ease when compared to a purely visual display. Added advantages of haptic simulators include increased repeatability, scalability, safety, and control over environmental conditions. It is also possible to simulate additional physical forces and fields, which may or may not be part of a natural environment, to convey information to the user. This makes a haptic display suitable for a variety of applications like remote operation in hazardous environments, simulators for surgical training [6]–[8], and rehabilitation research [9]–[12]. Physical therapy utilizing the resistance offered to a user's motion during haptic interaction can be used for rehabilitation of impaired arm movements in patients. Furthermore, research has shown that augmented feedback presented in virtual environments accelerates the learning of motor tasks [11]. For these reasons, the authors have developed an arm exoskeleton that can be utilized for such training and rehabilitation applications.

A force-feedback exoskeleton is a haptic device worn by the user. Arm exoskeletons can simulate large forces at the hand or arm, like the weight of an object that is held. This is achieved by providing feedback to the various joints of the arm—the shoulder, elbow, and wrist. Although worn by the user, the device itself may be grounded, in which case it restricts user mobility. In the mid 1960s and early 1970s, a group of researchers at Cornell University and later at General Electric developed some of the earliest master-slave teleoperation systems, the Handyman and Hardiman [13]. The Hardiman was an anthropomorphic exoskeleton placed inside a larger slave robot, and was used to amplify human power output. Input commands from the user were obtained from both the arms and legs. These early exoskeleton haptic devices were hampered by limitations in actuation, computation, and control systems technology. The reader is encouraged to review [1] for an exhaustive discussion of the early stages of exoskeleton and haptic interface development.

In recent years, improvements in sensing and actuation technologies, control systems, and computing resources have led to development of many successful haptic interfaces. Although there have been a large number of high-performance hand controllers, research in design of exoskeletons for other parts of the body is still in an early phase. The first modern exoskeleton

Manuscript received June 16, 2004; revised February 19, 2005. Recommended by Technical Editor C. Mavroidis.

The authors are with the Mechatronics and Haptic Interfaces Laboratory, Mechanical Engineering and Materials Science, Rice University, Houston, TX 77005-1892 USA (e-mail: abhi@rice.edu; omalleym@rice.edu).

Digital Object Identifier 10.1109/TMECH.2006.875558

arm/glove was designed and developed at ARTS laboratory for the replication of sensations of contacts and collisions [4]. The ARTS arm, also known as the PERCRO exoskeleton, is a 7-DOF ungrounded device, attached to the operator's shoulder and torso. The operator holds onto the device with his/her palm. Hence, the device can only exert forces at the palm of the user. It uses dc motors with a cable transmission system for actuation. A 9-DOF under-actuated exoskeleton arm developed at the Korea Institute of Science and Technology (KIST) by Lee *et al*. addressed the workspace issues associated with the PERCRO exoskeleton. Their device allows for full reproduction of the human arm's workspace when operating the exoskeleton [14]. A revised exoskeleton device from the same group employs electrical brakes in place of pneumatic actuators for improved bandwidth [15]. An alternate arm exoskeleton developed at KIST addresses the limited wearability issues of previous designs by using parallel mechanisms and pneumatic actuators [16]. The wearable Salford arm addresses some of the issues and limitations of earlier designs [5]. For example, nearly 90% of the human arm's workspace can be replicated with their device. Pneumatic muscle actuators (pMAs) were selected to power the robot due to their high power-to-weight ratio. A drawback of this choice is the highly nonlinear behavior and slow response of the pMAs, presenting additional control challenges.

Several human power amplifier systems, related to exoskeleton haptic devices, have been presented in the literature [17]–[19]. Human amplifier systems provide force feedback to the operator through a direct coupling between the amplification device and the operator. While there are some overlapping design considerations between human amplification systems and exoskeletons, there are also unique considerations for each. For example, with power-assisted systems, the operator directly receives feedback from a natural environment, and the device allows the user to achieve greater power output than can be achieved by a human alone. Conversely, a haptic exoskeleton must provide force feedback and simultaneously allow interactions with simulated environments. Many environment-rendering methods impose design constraints for these haptic exoskeletons that will be discussed throughout this paper.

Force control of arm exoskeletons is traditionally implemented under the assumption of pseudostatic operation (see, for example, [4]). In this approach, the robot Jacobian can be used to compute required actuator torques for some desired force at the end-effector. Recently, Rosen *et al*. presented some interesting results with the use of myosignals, command signals sent to the human muscles by the brain, in predicting human arm motion during operation of a single-DOF arm exoskeleton [20]. They showed that the prediction of operator motion can be used to improve upon the force control and overall quality of the haptic device.

Many prior exoskeleton interfaces attempt to optimize one or more of the following characteristics of the haptic system, namely power-to-weight ratio [5], [14], [16], workspace [14], wearability [16] or stability, and control bandwidth [4], [21], [22]. Individual designs, however, achieve these optimizations at the expense of other useful features, usually workspace [4], [16], [21] or control bandwidth [5], [14], [16]. In this paper, the authors present work that combines the useful results from prior research toward the design of a high-quality haptic interface with a workspace comparable to that of human arm workspace. This is achieved at the expense of added weight and decreased mobility due to device grounding. Fig. 1 shows a subject operating the proposed exoskeleton.

Fig. 1. User operating the exoskeleton.

II. Background

Haptic feedback aids an operator to reliably complete a remote or virtual task. Primary requirements for such a system are the ability to convey commands to the remote or virtual plant and to reflect relevant sensory information, specifically forces in the remote or virtual environment, back to the operator. In essence, the dynamics of the device must not interfere with the interaction between the operator and environment. An ideal haptic interface behaves as a rigid body, through which the user interacts with the environment, over the complete range of frequencies of forces in the virtual environment.

In practice, however, performance is limited by physical factors, such as actuator and sensor quality, device stiffness, friction, device workspace, force isotropy across the workspace, backlash, and computational speed. Force isotropy, which refers to the equality of force exertion capability of the device in all directions, is important to ensure consistent device performance across the workspace. The desired size and shape of the workspace itself is typically dependent on the target application, and serves as an important factor in determining the overall device size and mechanism. Increased workspace is only achieved at the expense of a larger and heavier device, since the force output requirements scale with the workspace size. Also of consideration in the design of haptic arm exoskeletons is the biomechanics of the human arm. The arm imposes a force/position constraint on the device, thus affecting the system behavior and performance. These design factors are discussed in detail in Sections II-A–II-C.

A. Biomechanics of Human Arm

A haptic arm exoskeleton places kinematic constraints on the human arm. The human arm has seven DOF: Abduction/adduction and flexion/extension of the shoulder; rotation of the upper arm; flexion/extension of the elbow; rotation of the forearm; and radial/ulnar deviation and flexion/extension

TABLE I
COMPARISON OF WORKSPACE AND TORQUE LIMITS OF HUMAN ARM AND EXOSKELETON JOINTS

Joint	Human Isometric Strength[1]	Human Joint Workspace Limits	Torque Specification	Workspace Specification	Peak Torque Output Capability	Workspace Capability
Elbow Flexion/Extension	72.5 Nm	Flexion: 146° Extension: 0°	6 Nm	Flexion: 120° Extension: 0°	5.46 Nm	Flexion: 90° Extension: 0°
Forearm Supination/Pronation	9.1 Nm	Supination: 86° Pronation: 71°	5 Nm	Supination: 90° Pronation: 90°	5.08 Nm	Supination: 90° Pronation: 90°
Wrist Palmar/Dorsal Flexion	19.8 Nm	Palmar Flexion: 73° Dorsiflexion: 71°	4 Nm	Palmar Flexion: 60° Dorsiflexion: 60°	≈ 0.4 Nm @ $\alpha = 30°; \beta = 9°$	Palmar Flexion: 60° Dorsiflexion: $> 60°$
Wrist Abduction/Adduction	20.8 Nm	Adduction: 33° Abduction: 19°	4 Nm	Adduction: 30° Abduction: 30°	≈ 0.4 Nm @ $\alpha = 21°; \beta = -11°$	Adduction: 30° Abduction: $> 30°$

of the wrist. It is desirable that the haptic exoskeleton does not compromise with the natural arm motion and workspace of the operator. The device should also have torque capabilities to match and enhance human abilities. Table I shows the workspace and torque capabilities of the human arm for reference.

B. Performance-Related Design Parameters

A high-quality haptic interface is characterized by stability robustness and transparency. The stability bandwidth refers to the range of frequencies of forces that can be reflected to the operator with the device, while ensuring stable system behavior. Research has shown that stability of a haptic simulation is related to the simulation rate, virtual wall stiffness, and device viscosity [23]. Transparency is a measure of the degree of distortion between the force at the human–robot interface and the desired contact force as commanded through the virtual environment. Transparency can be degraded by such things as backlash, inertia, or friction in the haptic device, sensor resolution, and computational delay [24]. Often with haptic interfaces, the quality of the device is characterized by the maximum virtual wall stiffness that can be stably displayed.

C. Control-Related Design Parameters

A haptic system applies trajectory-dependent forces to the operator's body. This is typically implemented in one of two modes—the impedance control mode and the admittance control mode. Impedance control techniques measure position at the human–machine interface and in turn adjust the commanded force at the human–machine interface depending on the virtual environment model to be displayed. It is desirable that an impedance-controlled haptic device allows free movement in response to the operator's motion commands, so that when the human is moving in free space (not in contact with any virtual objects), there is no resistance to motion. This requirement translates to a need for backdrivability in impendence-controlled haptic devices. In this control mode, it is also desirable for the device to have minimal inertia to facilitate maneuvering. Furthermore, low inertia and friction improve interface performance by reducing the forces required to compensate for device dynamics. Alternatively, admittance control methods rely on measurement of forces at the human–machine interface and controlled robot motion based on the virtual environment model. An admittance-controlled haptic device should prevent movement of the robot in response to operator-generated forces to allow for consistent force measurement and motion control.

It is apparent that haptic exoskeleton design involves various tradeoffs, which limit the achievable performance of the device since, in all instances, stability must be maintained. To summarize these tradeoffs, mechanism design choices may limit or affect human motion abilities; sensor and actuator selection is directly related to device weight, force output range, system stability, and cost; and actuator placement and inclusion of transmissions affects the apparent inertia of the device. All of these design decisions are greatly influenced by the intended application for the device.

III. METHODS

The MAHI exoskeleton, named for the Mechatronics and Haptic Interfaces Lab at Rice University, has been designed primarily for training and rehabilitation in virtual environments. These applications typically require the use of virtual force fields for guidance [25] or active assistance [26], [27]. The exoskeleton device must therefore allow natural human arm movements, with minimal reduction in workspace of the human arm. Because the device is to be worn, special care must be taken to ensure safety of the wearer. Furthermore, mobility of the interface is not normally a requirement for such a system. Hence, the device can be grounded to support excessive weight, and gravity compensation can be implemented through the controller. Additionally, the low accelerations and velocities associated with human movements ensure that the inertia of the device plays a small role in its operation [4], [28]. Therefore, when designing the MAHI exoskeleton, the kinematic design of the robot has been given prime consideration.

Table I shows the desired design specifications for the exoskeleton in terms of the range of motion and torque display capability. The workspace specifications closely match the average range of motion of human joints. The torque capabilities lag far behind human abilities due to the limitations in the current actuator technology and some practical restrictions on the size of actuators, which can be used in an arm exoskeleton. The torques achieved by Tsagarakis *et al*. [5] have been used as target specifications for design. Tsagarakis *et al*. employ pMAs with a tendon-based transmission for their exoskeleton design. This allows their exoskeleton to achieve high torque output and a larger workspace compared to prior arm exoskeleton systems. The disadvantage of using pneumatic actuation is the low bandwidth

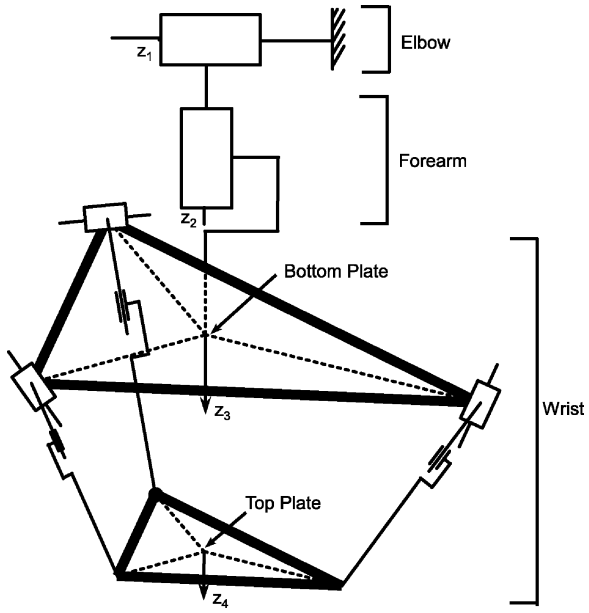

Fig. 2. Exoskeleton mechanism: A 3-RPS platform is used as the wrist of the robot. Joints R_1, R_2, and R_3 and B_1, B_2, and B_3 are located at vertices of equilateral triangles.

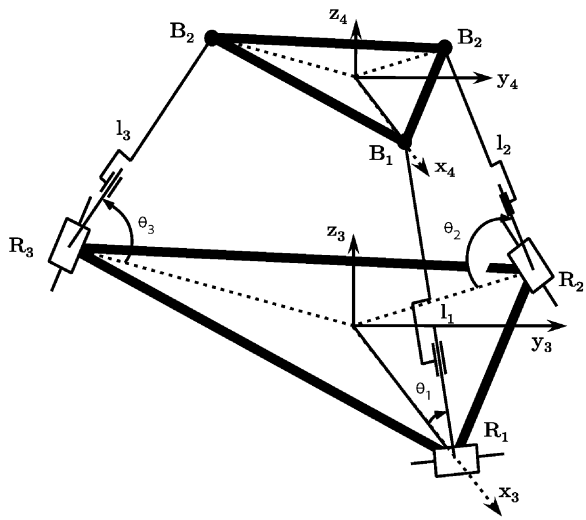

Fig. 3. 3-RPS platform (adapted from [31]).

of the actuators and the requirement of delicate control due to their nonlinear behavior. Because the MAHI exoskeleton uses electric actuators, with lower power-to-volume and power-to-weight ratios than pneumatic actuators, the authors feel that the torque requirements of Tsagarakis serve as a challenging benchmark.

Research has shown that fairly low stiffness and force values are sufficient for object detection [29], [30]. Therefore, if a haptic exoskeleton is designed for teaching arm movements using virtual force fields, a low force output interface would suffice. In this case, as the authors intend for the device to be used as a general purpose training tool for arm movements, it is required that the device be able to simulate high-quality virtual surfaces. As a result, emphasis is placed on the design of a high-performance interface, which encompasses the human arm workspace. In addition, for rehabilitation applications, the ability to control feedback to individual human arm joints is desirable and has been addressed through this design.

IV. Results

A. Basic Mechanism Design

The basic kinematic structure of the 5-DOF MAHI exoskeleton is depicted in Fig. 2. The exoskeleton is comprised of a revolute joint at the elbow, a revolute joint for forearm rotation, and a 3-revolute-prismatic-spherical (RPS) serial-in-parallel wrist.

The 3-RPS platform, mentioned by Lee and Shah [31], consists of a base plate, three extensible links l_1, l_2, and l_3, and a moving platform, as shown in Fig. 3. The moving platform houses the end-effector that is affixed to the operator during operation. The moving platform is connected to the three extensible links by means of spherical joints spaced at 120° along the circumference of a circle of radius r. The other end of the links connects to the base platform via revolute (pin) joints, which are also spaced 120° along a circle of radius R. The axes of rotation of the revolute joints are oriented along the tangents to the circle of radius R. Linear actuators placed along the link are used to change the link length, thereby moving the top platform. It should be noted that the platform has limited movement transverse to the vertical axis through the base and no singularities for $\theta_i \in (0, \pi)$ [31].

The choice of a parallel mechanism for the design of the exoskeleton wrist over a serial mechanism was motivated primarily by the compactness of the parallel mechanism. Furthermore, use of a parallel mechanism allows for higher torque output, stiffness, and decreased inertia compared to a similar serial mechanism.

During operation, the robot is worn so that the axis elbow joint of the robot aligns with the operator's elbow joint, and the top plate of the wrist of the robot aligns with the wrist joint of the operator. This configuration aids in preserving natural arm movements by aligning the robot's kinematic structure with that of the human arm. Velcro strapping and an ergonomic palm splint are used to maintain this alignment. The mapping between the robot configuration and arm position is further simplified by the use of the 3-RPS kinematic structure for the robot. The equivalence between the human wrist joint angles and the xyz Euler angle representation for the orientation of the platform is shown in Section IV-E.

B. MAHI Exoskeleton Kinematics

For the purpose of analysis, the coordinate axes are fixed to various joints of the exoskeleton, as shown in Fig. 2. Frames $\{1\}$ and $\{2\}$ are fixed to the ground and elbow joints, respectively, whereas frames $\{3\}$ and $\{4\}$ are fixed to the plates of the platform.

The transformation matrices between frames $\{1\}$ and $\{2\}$ and $\{2\}$ and $\{3\}$ are given by

$$ {}^{1}\mathbf{T}_{2} = \begin{bmatrix} \cos\theta_4 & -\sin\theta_4 & 0 & 0 \\ \sin\theta_4 & \cos\theta_4 & 0 & 0 \\ 0 & 0 & 1 & 0 \\ 0 & 0 & 0 & 1 \end{bmatrix} \tag{1} $$

$$ {}^{2}\mathbf{T}_{3} = \begin{bmatrix} \cos\theta_5 & -\sin\theta_5 & 0 & 0 \\ \sin\theta_5 & \cos\theta_5 & 0 & l \\ 0 & 0 & 1 & 0 \\ 0 & 0 & 0 & 1 \end{bmatrix} \tag{2} $$

where θ_4 and θ_5 are the angles of rotation of the elbow and forearm joints and $(0, l, 0)^T$ is the location of the center of the base plate of the platform in $\{2\}$.

Now, given the transformation matrix between frames $\{3\}$ and $\{4\}$, the position and orientation of the wrist platform can be computed, which provides the position and orientation of the human wrist. Section IV-C presents in detail the kinematics of the wrist. The elbow and forearm joints of the robot and human being coincident, the measurement of position of operator's elbow and forearm from robot coordinates and vice versa is trivial as shown in Section IV-A.

C. Kinematics of the Wrist Mechanism

As shown in Fig. 3, the base coordinate frame $\{3\}$ is attached to the center of the base platform with the z_3-axis pointing vertically upward and x_3-axis toward the first revolute joint R_1. Frame $\{4\}$ is attached to the moving platform with the z_4-axis being normal to the platform and the x_4-axis pointing toward the first spherical joint B_1. Using Grashoff's criterion it can be shown that the system has three DOF. Furthermore, due to the constraint imposed by the revolute joints, the rotation of the platform about z_4-axis is not possible. Hence, the platform has only two DOF in orientation and one in translation. The length of individual links are denoted by l_i. The coordinates of the revolute joints relative to $\{3\}$ are

$$ \boldsymbol{R}_1 = \begin{bmatrix} R \\ 0 \\ 0 \end{bmatrix} \quad \boldsymbol{R}_2 = \begin{bmatrix} \frac{-1}{2}R \\ \frac{\sqrt{3}}{2}R \\ 0 \end{bmatrix} \quad \boldsymbol{R}_3 = \begin{bmatrix} \frac{-1}{2}R \\ \frac{\sqrt{3}}{2}R \\ 0 \end{bmatrix} \tag{3} $$

and the coordinates of the spherical joints in $\{4\}$ are

$$ {}^{4}\boldsymbol{B}_1 = \begin{bmatrix} r \\ 0 \\ 0 \end{bmatrix} \; {}^{4}\boldsymbol{B}_2 = \begin{bmatrix} \frac{-1}{2}r \\ \frac{\sqrt{3}}{2}r \\ 0 \end{bmatrix} \; {}^{4}\boldsymbol{B}_3 = \begin{bmatrix} \frac{-1}{2}r \\ \frac{\sqrt{3}}{2}r \\ 0 \end{bmatrix}. \tag{4} $$

The homogeneous transformation matrix ${}^{4}T_3$, which represents $\{4\}$ in terms of the base frame $\{3\}$, is

$$ {}^{3}\mathbf{T}_{4} = [\boldsymbol{n} \quad \boldsymbol{o} \quad \boldsymbol{a} \quad \boldsymbol{p_c}] \tag{5} $$

where $\boldsymbol{p_c} = (x_c, y_c, z_c)^T$ denotes the position of the origin of frame $\{4\}$ in the base frame. The direction cosines of the unit vectors x, y, and z in the base frame are represented by $\boldsymbol{n} = (n_1, n_2, n_3)^T$, $\boldsymbol{o} = (o_1, o_2, o_3)^T$, and $\boldsymbol{a} = (a_1, a_2, a_3)^T$. For subsequent analysis, all coordinates and lengths have been normalized using the base radius R. The following are defined:

$$ \rho = \frac{r}{R} \quad L_i = \frac{l_i}{R} $$

then

$$ X_c = \frac{x_c}{R} \quad Y_c = \frac{y_c}{R} \quad Z_c = \frac{z_c}{R}. $$

1) Forward Kinematics: The forward kinematics for the platform involves solving simultaneous equations for the position and orientation of the movable platform in terms of the given link lengths. The fact that the manipulator is essentially a structure for fixed lengths has been used to derive these equations. If θ_i is the angle between link R_iB_i, then coordinates of the spherical joints with respect to the base frame are

$$ {}^{3}\boldsymbol{B}_i = \begin{bmatrix} \cos\left(\frac{(i-1)2\pi}{3}\right)(1 - L_i\cos\theta_i) \\ \sin\left(\frac{(i-1)2\pi}{3}\right)(1 - L_i\cos\theta_i) \\ L_i\sin(\theta_i) \end{bmatrix}, \quad i = 1, \ldots, 3. \tag{6} $$

The distance between any two spherical joints $\sqrt{3}r$ can be used to implicitly relate θ_i to L_i. This leads to three constraint equations given by (7)–(9)

$$ \begin{aligned} &L_1^2 + L_2^2 - 3 - 3\rho^2 + L_1L_2\cos\theta_1\cos\theta_2 \\ &\quad - 2L_1L_2\sin\theta_1\sin\theta_2 - 3L_1\cos\theta_1 \\ &\quad - 3L_2\cos\theta_2 = 0 \end{aligned} \tag{7} $$

$$ \begin{aligned} &L_3^2 + L_2^2 - 3 - 3\rho^2 + L_3L_2\cos\theta_3\cos\theta_2 \\ &\quad - 2L_3L_2\sin\theta_3\sin\theta_2 - 3L_3\cos\theta_3 \\ &\quad - 3L_2\cos\theta_2 = 0 \end{aligned} \tag{8} $$

$$ \begin{aligned} &L_1^2 + L_3^2 - 3 - 3\rho^2 + L_1L_3\cos\theta_1\cos\theta_3 \\ &\quad - 2L_1L_3\sin\theta_1\sin\theta_3 - 3L_1\cos\theta_1 \\ &\quad - 3L_3\cos\theta_3 = 0. \end{aligned} \tag{9} $$

Multiple solutions of θ_1, θ_2, and θ_3 for a given set of link lengths are possible. A further mathematical constraint $0^\circ < \theta_i < 180^\circ$ ensures uniqueness. In other words, the position z_c for the platform must always be positive, i.e., the moving platform should always move on one side of the base platform, a physical constraint. With this constraint, (7)–(9) can be solved numerically for θ_i. As the spherical joints are placed at the vertices of an equilateral triangle, the Cartesian position of the origin of the moving frame $\{4\}$, which is the centroid of the triangle, C can be computed as

$$ \boldsymbol{P_c} = [X_c \quad Y_c \quad Z_c] = \frac{1}{3}\sum_{i=1}^{3}\frac{\boldsymbol{B}_i}{R}. \tag{10} $$

Using (4), the Cartesian position of the spherical joints can be expressed as

$$ \begin{bmatrix} {}^{4}\boldsymbol{B}_i \\ 1 \end{bmatrix} = {}^{4}T_3 \begin{bmatrix} {}^{3}\boldsymbol{B}_i \\ 1 \end{bmatrix}. \tag{11} $$

Equations (11) and (6) can be solved to determine the vectors $\boldsymbol{n}$, $\boldsymbol{o}$, and $\boldsymbol{a}$, and hence the orientation of the platform. The components of $\boldsymbol{n}$ are determined by equating the Cartesian position of spherical joint B_1 from the above-mentioned equations

$$n_1 = \frac{1 - L_1 \cos\theta_1 - X_c}{\rho} \quad n_2 = -\frac{Y_c}{\rho}$$
$$n_3 = \frac{L_1 \sin\theta_1 - Z_c}{\rho}.$$

Similarly, equating B_2 from (6) and (11), the vector $\mathbf{o}$ is

$$o_1 = n_2 \quad o_2 = \frac{\sqrt{3} - \sqrt{3}L_2 \cos\theta_2 - 3Y_c}{\sqrt{3}\rho}$$
$$o_3 = \frac{2L_2 \sin\theta_2 + L_1 \sin\theta_1 - 3Z_c}{\sqrt{3}\rho}.$$

As the unit vectors $\boldsymbol{n}$, $\boldsymbol{o}$, and $\boldsymbol{a}$ are orthogonal, $\mathbf{a}$ is determined as

$$a_1 = n_2 o_3 - n_3 o_2 \quad a_2 = n_3 o_1 - n_1 o_3 \quad a_3 = n_1 o_2 - n_2 o_1.$$

Once the transformation matrix $\mathbf{T}$ is known, the orientation of the platform in terms of xyz-Euler angles, α, β, and γ, can be determined using

$$\beta = \sin^{-1}(n_3) \quad \alpha = A\tan 2(-o_3/\cos(\beta), a_3/\cos(\beta))$$
$$\gamma = A\tan 2(-n_2/\cos(\beta), n_1/\cos(\beta)).$$

It should be noted that if $\beta = \pm 90^\circ$, α and γ become indeterminate. In addition, the top plate of the platform cannot rotate about z_4, and hence, $\gamma = 0$ in general.

2) Inverse Kinematics: As the moving platform has three DOF, its position can be defined in terms of the first two xyz-Euler angles, α and β, and one Cartesian coordinate, Z_c. As the links R_1B_1, R_2B_2, and R_3B_3 are constrained by the revolute joints to move in the planes $y = 0, y = -\sqrt{3}x$, and $y = \sqrt{3}x$, respectively, using (11) we have

$$n_2\rho + Y_c = 0; \quad X_c = \frac{\rho}{n_1 - o_2}.$$

Now, $\gamma = 0$, as the top plate of the platform cannot rotate about z_4. Hence, X_c, Y_c, and γ can easily be solved. The orientation and position of the top plate can then be used to compute the transformation matrix $\mathbf{T}$ and determine the Cartesian positions $\boldsymbol{B}_i$ using (11). The actuator position is then trivial to calculate as the length of link R_iB_i.

D. Kinematic Design of the Wrist

The 3-RPS platform used as the wrist platform involves several design parameters, which affect the workspace of the device. These parameters are the ratio of the radii of the top and base platforms ρ, the link travel, the maximum link length, and the height of the platform. The parameters were calculated using the sequential quadratic programming algorithm, to optimize the wrist workspace for $\pm 60^\circ$ in pitch (rotation about y_4) and $\pm 30^\circ$ in yaw (rotation about x_4). The algorithm is implemented through the fminimax function as a part of the MATLAB optimization toolbox.

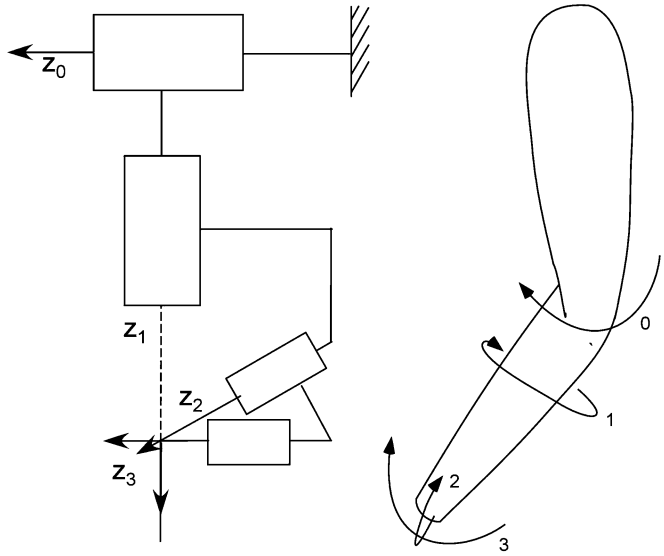

Fig. 4. Simplified kinematic model of the human arm (other axes have not been shown for clarity). Axes 0 through 3 represent elbow rotation, forearm rotation, elbow adduction/abduction, and elbow flexion/extension, respectively.

The wrist platform dimensions were determined via design optimization, with ρ and platform height as the variables to be selected. A weighted sum of the maximum link length and link travel was chosen as the cost function to be minimized, and is given as

$$f(x) = L_{\max}^2 + (L_{\max} - L_{\min})^2 \tag{12}$$

where $L_{\max}$ and $L_{\min}$ are the maximum and minimum link lengths over the entire workspace of interest. It should be noted that the height of the platform is maintained constant during operation of the exoskeleton, as only the two DOF of orientation of the top plate are utilized. The sizes of the human wrist and elbow provide constraints on the diameter of the top and base plates of the platform. In addition, the base of the platform can collide with the ground links at the upper arm during elbow flexion, thus limiting the workspace. Therefore, it is desirable that the height of the platform and the travel of the links be kept to minimum, so that the base is as close to the human wrist as possible.

E. Measurement of Human Wrist Joint Angles

A simplified kinematic model of the human lower arm and the wrist is shown in Fig. 4. Note that axes x_4 of the platform (see Fig. 3) and z_2 of the human wrist joint coincide when the exoskeleton is worn by an operator. Similarly, axes y_4 of the platform and z_3 of the arm coincide for any rotation α of the top plate of the platform about x_4, or of the human wrist about z_2 (Fig. 4). Furthermore, $\{3\}$ of the platform has a fixed orientation with respect to $\{1\}$ of the human arm. Hence, a rotation of the top plate of the platform about x_4-axis (Fig. 3) followed by another rotation about y_4-axis (Fig. 3), is equivalent to a transformation from $\{3\}$ to $\{1\}$ of the arm. This implies that with the top plate of the platform centered at the operator's wrist joint, the measurement of the orientation of the top plate with respect to the base of the platform in terms of xyz-Euler angles corresponds to measurement of the flexion/extension and abduction/adduction of the

TABLE II
SENSOR AND ACTUATOR SPECIFICATIONS

Axis	Peak Output Force/Torque	Peak Stall Force/Torque	Sensor Resolution	Remarks
Elbow Flexion/Extension	5.459 Nm	0.487 Nm	0.175°	Actuator : Kollmorgen U9D-E Encoder : US Digital E3-2048-500-H
Forearm Supination/Pronation	5.08 Nm	1.694 Nm	0.002°	Actuator : Applimotion 165-A-18 Encoder : MicroE Systems Mercury 1500
Linear Axes	9.5 N	3.19 N	1um	Actuator : Copley Controls TB1102 Encoder : Renishaw RGH24

human wrist joint. Therefore, xyz-Euler angle representation of $\{4\}$ relative to $\{3\}$ is used for the orientation of the platform for subsequent analysis. The Euler angle of rotation α about x_4-axis corresponds to abduction/adduction of the wrist while the rotation angle β about y_4-axis corresponds to flexion/extension.

F. Sensing and Actuation

1) Sensor Selection: Sensor resolution affects the range of frequencies of forces that can be displayed by the haptic interface [24]. Consider, for example, the simulation of a thin virtual wall. If the sensor resolution or the computational speed is not high enough, then there exists a possibility that the human can pass his/her arm through the wall without feeling the force. Furthermore, during simulation of stiff virtual surfaces, reduction in sensor resolution increases the delay in sensing the human's actions in the virtual environment, and this delay can decrease system stability. With these considerations, high resolution optical encoders were selected for the device.

2) Actuator Selection: The actuators for a haptic device determine the range of magnitude and frequencies of forces that can be displayed with the interface. To reproduce real-life environments, it is desirable that the device be able to display forces in a large range of magnitudes as well as frequencies. In general, the use of high-power actuators is accompanied with an increase in weight, thereby increasing the inertia of the device. Thus, high power-to-weight ratio and high bandwidth are desirable qualities for actuators used in a haptic interface. The bandwidth refers to the dynamic response of the actuator; a low-bandwidth actuator fails to display high-frequency forces to the operator, reducing system transparency in such situations. This gains importance in that human kinesthetic/preprioceptic sensing bandwidth is 20–30 Hz and tactile sensing bandwidth is 0–400 Hz [28].

No single actuator technology provides the benefit of both high power-to-weight ratio and high bandwidth. Pneumatic actuators are inexpensive and provide the benefit of high power-to-weight ratio. However, pneumatic actuators have a low bandwidth, which limits their utility as actuators for haptic interfaces. Tsagarakis *et al*. used pMAs for their exoskeleton [5]. However, these actuators have highly nonlinear dynamics in addition to low bandwidth, making them unsuitable for application in haptic devices. Hence, electrical actuation was chosen for the MAHI exoskeleton. Electrical actuators have a lower power-to-weight ratio than pneumatic actuators but have very high bandwidth. This increases the weight of the device but allows for better force reflection through the interface. Table II lists the specifications for the sensors and actuators used for the exoskeleton.

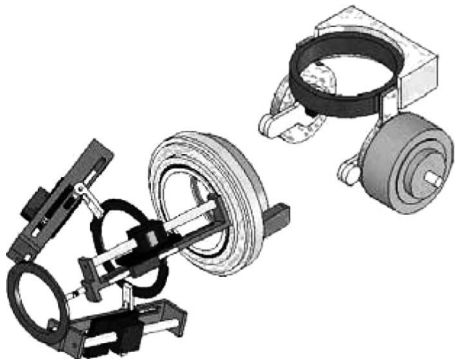

Fig. 5. Exploded view of exoskeleton assembly.

3) Transmission and Actuator Placement: A transmission can be used to increase the torques or forces delivered by the device, but at the expense of speed of operation. The bandwidth of human motor output, which represents the ability of the hand and fingers to exert forces, is 10–15 Hz [28], thus making the use of a transmission in haptic interfaces advantageous. Furthermore, use of a transmission allows the actuators themselves to be placed closer to the base of the robot, reducing rotational inertia.

Use of transmissions, however, is associated with tradeoffs like backlash, nonlinear dynamics, and complex cable routing. For example, gears introduce backlash into the system, whereas cable and belt drives introduce nonlinearities. Additionally, in arm exoskeleton design, use of cable or belt drives involves complex routing to ensure hindrance-free arm operation. Bergamasco *et al*. used a cable drive to power their exoskeleton and reported the routing of cables to be a major part of the design process [4]. The parallel wrist mechanism used in our design can further magnify this problem. For these reasons, a direct drive mechanism was selected. This simplifies device design and ensures optimal transparency and performance. The drawbacks include a reduction in the magnitude of forces that can be displayed through the device. As a result, the current design of the exoskeleton cannot compensate for gravitational effects throughout the workspace of the device. Another drawback of direct-drive actuation is increased inertia. Frameless electrical actuators were selected to keep the increase in inertia to a minimum.

G. Assembly of the Exoskeleton

An exploded view of the robot assembly is shown in Fig. 5. The device uses frameless electrical motors for forearm and wrist joints and is made almost entirely of aluminum. Due to the

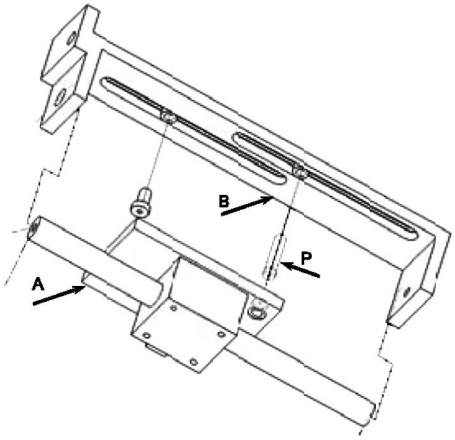

Fig. 6. Platform link mechanism: Link A carries the linear actuator block and rotates about pin P; Link B acts as the prismatic link of the wrist platform. Links A and B are mechanically coupled for synchronous rotation and B can translate with respect to both A and P.

use of frameless actuators, the amount of material required for construction was tremendously reduced. Aluminum has been used for construction over lightweight polymers like carbon fiber for several reasons.

1) Aluminum has much higher stiffness than polymers.
2) Polymers like carbon fiber are typically stronger under axial loading than transverse.
3) Being metallic, aluminum components are conducive to the performance of frameless motors.

Design of the wrist platform required extra considerations due to the use of electric actuation. Unlike variable length pneumatic actuators, the electric actuators used have a fixed total length. Therefore, the revolute joint was replaced with a cylindrical joint with the same axis of rotation (see Fig. 6). Both links A and B can rotate about the axis of rotation through pin P, whereas link B can also slide over pin P, thus making the cylindrical joint. Bearings have been used in the slots to reduce friction and backlash.

The range of motion of the spherical joint at the movable plate of the platform limits the workspace of platform. Equations developed by Lee and Shah were used to compute the range of rotations required from the spherical joint to meet our workspace criteria [31]. It was found that commercially available spherical joints do not suffice to meet the workspace requirements. Hence, the spherical joint was replaced with a 4-DOF spherical joint between the top plate of the platform and the corresponding linear joint links. This joint consisted of a universal joint attached at either end to the link and the moving platform via rotary joints. This adds redundancy to the system and permits larger rotations. For the purpose of kinematic analysis, the redundancy does not affect any of the geometric relations or equations.

H. Safety and Comfort

During the design process, precedence was given to compactness of the design and robot kinematics. A direct drive mechanism was used to avoid backlash and nonlinearities associated with transmissions. As a result, the MAHI exoskeleton weighs more than 4 kg. Therefore, the device was grounded to the wall to reduce discomfort to the user.

The workspace of the exoskeleton is greater than the workspace of the human arm for some joints (see Table I). In such circumstances, hardware stops in conjunction with software limits have been used to ensure user safety. Emergency stop switches are also provided.

V. Discussion

This paper presents the mechanical design of a haptic arm exoskeleton that uniquely balances design tradeoffs inherent in haptic exoskeleton device design. The proposed mechanism allows for a compact robot design, centered around the human arm. Table I shows the torque and workspace capabilities of the exoskeleton.

It can be seen that the exoskeleton design meets the desired workspace specifications for all joints except the elbow joint. The device is capable of 90° of elbow extension, which is approximately 30° less than the design specification. The range of motion achievable with the exoskeleton during elbow flexion is limited because the base of the wrist platform collides with the ground links at the upper arm at the extents of elbow flexion. It should be noted that the achievable elbow workspace is sufficient for many common tasks. The human forearm and wrist capabilities are listed in Table I. As can be seen, the exoskeleton does not compromise the operator's forearm rotation or abduction/adduction of the wrist. Almost 90% of wrist the workspace can be reproduced in flexion/extension. Furthermore, the 3-RPS platform allows for compact design, centered on the human arm, which increases wearability and maximizes the achievable workspace of the exoskeleton. An increase in the wrist workspace can be achieved by reduction of ρ, the ratio of radii of top and base plates of the platform, or increase in the height of the platform. Reduction in ρ by decreasing the radius of top plate is limited by the size of the operator's wrist, whereas, both reduction in ρ through increase in the radius of the base plate or increase in the height of the platform would further compromise elbow workspace.

In terms of torque reproduction capabilities, the peak torque output of the exoskeleton meets the design requirements for the elbow joint and for the rotation of the human forearm. The specifications for torque feedback to the wrist, however, could not be met owing to actuator limitations and the use of direct drive actuation. Direct drive actuation has been used to simplify design and reduce backlash and slip, which helps to verify the function of the kinematic design. However, this prevents gravity compensation when the device is in operation, as the continuous torque output capabilities of the actuators are much less than their corresponding peak torque output limits. This is a consequence of the fact that peak current ratings of electrical motors are lower than the continuous current ratings.

One important feature of the exoskeleton design is the alignment of the axes of the rotation of human joints with the controlled DOF of the exoskeleton. The problem of measurement of arm position is thus reduced to the solution of the exoskeleton kinematics, with no further transformations required as was

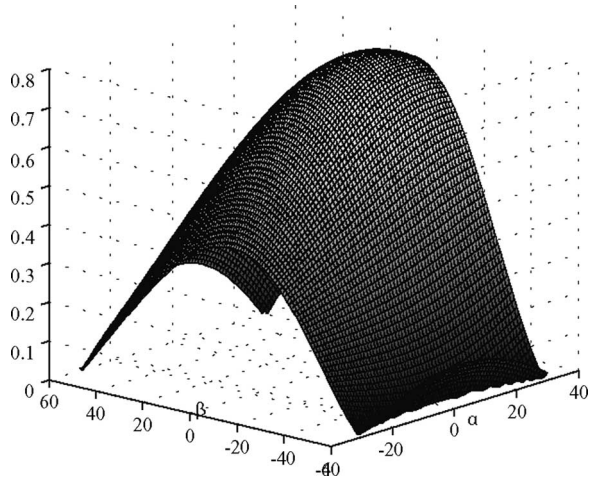

Fig. 7. Manipulability of the wrist mechanism: α, abduction/adduction; β, flexion/extension.

for some prior designs, for example [14], [15]. In addition, this makes it possible to actuate the robot to provide feedback to a specific human joint, for example, to constrain the forearm rotation during wrist rehabilitation, without affecting other joints. This is a distinct advantage over some of the other exoskeletons presented in literature, for example [4], [14], [15], [22], for which only the endpoint force can be regulated. This is particularly relevant for rehabilitation purposes, where the therapist might desire to focus the therapy toward a particular joint. Fig. 7 shows the manipulability of the wrist platform measured as the absolute determinant of the inverse Jacobian [32]. Manipulability of a robot is a quantitative measure that captures the ease with which the device can arbitrarily change position and orientation from a given posture. For the MAHI exoskeleton, the manipulability measure is greatest in the center of the workspace, with the wrist at 0° of abduction/adduction (α) and flexion/extension (β). Manipulability, as expected, is low at the extents of each joint range of motion, although more so for flexion/extension. For the tasks of rehabilitation and training, it is expected that most useful interactions via the haptic device will take place away from the joint limits, and so manipulability should not limit device performance.

In addition to the aforementioned advantages due to the proposed 3-RPS mechanism, the device has minimal backlash, low friction, high backdrivability, high structural stiffness, and a singularity-free workspace. These features characterize a high-quality haptic interface. The absence of singularities in the workspace means that the forward and inverse kinematics of the robot can be solved uniquely at each point, thus making the measurement of arm position and force feedback easier. The use of electric actuators and high-resolution encoders also ensures desirable performance of the haptic interface.

VI. Conclusion and Future Work

This paper presents the first iteration of the design of a haptic arm exoskeleton for rehabilitation and training. The workspace of the robot encompasses almost 90% of the total human forearm workspace, except for the limitation in the flexion of the elbow joint. There exist no singularities in the workspace of the robot. The arm-centered design results in a compact interface that does not compromise natural arm movements. The alignment of human and robot axes permits easy measurement of human arm joint angles along with increased control over independent feedback to individual human arm joints. The device allows a trainer or therapist to provide customized feedback to individual joints. In addition, the system provides both mechanical as well as software safety features to provide a safe training environment for the user. The major limitation of the device is its torque output capability, which can be improved upon with the use of a transmission or counterbalanced links.

Future work related to the design of the MAHI exoskeleton will focus on design refinement and control. Specifically, a force controller capable of providing independent human arm joint force feedback will be implemented. Gravity compensation coupled with a capstan drive transmission for the elbow joint will be incorporated for improved device performance. The wrist platform will be analyzed and redesigned to achieve better torque characteristics. Finally, the exoskeleton interface will be used as a test bed for shared control as a means of training in haptic virtual environments [33].

References

[1] G. C. Burdea, *Force and Touch Feedback for Virtual Reality*. New York: Wiley, 1996.
[2] D. K. Boman, "International survey: Virtual-environment research," *Computer*, vol. 28, no. 6, pp. 57–65, Jun. 1995.
[3] S. D. Lay and A. M. Day, "Recent developments and applications of haptic devices," *Comp. Graph. Forum*, vol. 22, no. 2, pp. 117–132, 2003.
[4] M. Bergamasco *et al.*, "An arm exoskeleton system for teleoperation and virtual environment applications," in *Proc. IEEE Int. Conf. Robot. Automat.*, 1994, vol. 2, pp. 1449–1454.
[5] N. Tsagarakis, D. G. Caldwell, and G. Merdano-Cerda, "A 7DOF pneumatic muscle actuator powered exoskeleton," in *Proc. Int. Workshop Robot and Human Interact. Commun.*, 1999, pp. 327–333.
[6] C. R. Carignan and D. L. Akin, "Using Robots for Astronaut Training," *IEEE Control Syst. Mag.*, vol. 23, no. 2, pp. 46–59, Apr. 2003.
[7] D. Feygin, M. Keehner, and R. Tendick, "Haptic guidance: Experimental evaluation of a haptic training method for a perceptual motor skill," in *Proc. Int. Symp. Haptic Interfaces for Virtual Environ. Teleop. Syst.*, 2002, pp. 40–47.
[8] C. Basdogan, C.-H. Ho, and M. A. Srinivasan, "Virtual environments for medical training: Graphical and haptic simulation of laproscopic common bile duct exploration," *IEEE/ASME Trans. Mechatronics*, vol. 6, no. 3, pp. 269–285, Sep. 2001.
[9] G. M. Prisco *et al.*, "A virtual environment with haptic feedback for the treatment of motor dexterity disabilities," in *Proc. IEEE Int. Conf. Robot. Automat.*, 1998, vol. 4, pp. 3721–3726.
[10] D. Jack *et al.*, "Virtual reality enhanced stroke rehabilitation," *IEEE Trans. Neural Syst. Rehab. Eng.*, vol. 9, no. 3, pp. 308–318, Sep. 2001.
[11] E. Todorov, R. Shadmehr, and E. Bizzi, "Augmented feedback presented in a virtual environment accelerates learning of a difficult motor task," *J. Motor Behav.*, vol. 29, no. 2, pp. 147–158, 1997.
[12] H. Sveistrup. (2004). "Motor rehabilitation using virtual reality," *J. NeuroEng. Rehab* [Online]. *1*(*10*). Available: http://www.jneuroengrehab.com/info/about/
[13] R. S. Mosher, "From Handyman to Hardiman," *Soc. Automot. Eng. Trans.*, vol. 76, pp. 588–597, 1967.
[14] S. Lee *et al.*, "Design of a force reflecting master arm and master hand using pneumatic actuators," in *Proc. IEEE Int. Conf. Robot. Automat.*, 1998, pp. 2574–2579.
[15] Y. S. Kim *et al.*, "A force reflected exoskeleton-type masterarm for human-robot interaction," *IEEE Trans. Syst., Man, Cybern. A*, vol. 35, no. 2, pp. 198–212, Mar. 2005.

[16] Y. Jeong *et al*., "A 7 DOF wearable robotic arm using pneumatic actuators," in *Proc. Int. Symp. Robotics*, Seoul, Korea, Apr. 2006.
[17] H. Kazerooni and M.-G. Her, "The dynamics and controls of a haptic interface device," *IEEE Trans. Robot. Automat.*, vol. 10, no. 4, pp. 453–464, Aug. 1994.
[18] P. Y. Li, "Design and control of a hydraulic human power amplifier," in *Proc. ASME Int. Mechanical Engineering Congress Expo.*, Anaheim, CA, 2004.
[19] K. Kiguchi and T. Fukuda, "A 3 DOF exoskeleton for upper limb motion assist: Consideration of the effect of bi-articular muscles," in *Proc. IEEE Int. Conf. Robot. Automat.*, 2004, pp. 2424–2429.
[20] J. Rosen *et al*., "A myosignal-based powered exoskeleton system," *IEEE Trans. Syst., Man, Cybern. A*, vol. 31, no. 3, pp. 210–222, May 2001.
[21] A. Nakai, T. Oshashi, and H. Hashimoto, "7DOF arm type haptic interface for teleoperation and virtual reality systems," in *Proc. IEEE/RSJ Int. Conf. Intell. Robots Syst.*, Victoria, B.C., Canada, 1998, pp. 1266–1271.
[22] R. L. Williams II *et al*., "Kinesthetic force/moment feedback via active exoskeleton," in *Proc. Image Soc. Conf.*, Scottsdale, AZ, Aug. 1998.
[23] R. E. Elllis, O. M. Ismaeil, and M. G. Lipsett, "Design and evaluation of a high-performance haptic interface," *Robotica*, vol. 14, pp. 321–327, 1996.
[24] J. E. Colgate and J. M. Brown, "Factors affecting the Z-width of a haptic display," in *Proc. IEEE Int. Conf. Robot. Automat.*, 1994, pp. 3205–3210.
[25] L. Rosenberg, "Virtual fixtures: perceptual tools for telerobotic manipulation," in *Proc. IEEE Int. Symp. Virt. Reality*, 1993, pp. 76–82.
[26] B. Gillespie *et al*., "The virtual teacher," in *Proc. ASME Int. Mechanical Engineering Congress Expo.*, Anaheim, CA, Nov. 1998.
[27] M. K. O'Malley and A. Gupta, "Passive and active assistance for human performance of a simulated underactuated dynamic task," in *Proc. Int. Symp. Haptic Interfaces for Virtual Environ. Teleoperator Syst.*, 2003, pp. 348–355.
[28] K. Shimoga, "Finger force and touch feedback issues in dexterous telemanipulation," in *Proc. NASA-CIRSSE Int. Conf. Intell. Robotic System for Space Exploration*, Troy, NY, 1992, pp. 159–178.
[29] M. K. O'Malley and M. Goldfarb, "The effect of force saturation on the haptic perception of detail," *IEEE/ASME Trans. Mechatronics*, vol. 7, no. 3, pp. 280–288, Sep. 2002.
[30] ——, "The effect of virtual surface stiffness on the haptic perception of detail," *IEEE/ASME Trans. Mechatronics*, vol. 9, no. 2, pp. 448–454, Jun. 2004.
[31] K. M. Lee and D. K. Shah, "Kinematic analysis of a three degrees-of-freedom in-parallel actuated manipulator," *IEEE Trans. Robot. Automat.*, vol. 4, no. 3, pp. 354–360, Jun. 1988.
[32] T. Yoshikawa, "Manipulability of robotic mechanisms," *Int. J. Robot. Res.*, vol. 4, no. 2, pp. 3–9, 1985.
[33] M. K. O'Malley, "Shared control for upper extremity rehabilitation in virtual environments," in *Proc. ASME Int. Mechanical Engineering Congress Expo.*, Orlando, FL, 2005.

Abhishek Gupta (S'06) received the B.S. degree from the Indian Institute of Technology, Kharagpur, India and the M.S. degree from Rice University, Houston, TX, in 2001 and 2004, respectively, both in mechanical engineering. He is currently pursuing a Ph.D. degree, at Rice University.

His research interests include design and control of haptic interfaces, nanorobotic manipulation, and control of teleoperator systems.

Marcia K. O'Malley (S'00–A'01–M'03) received the B.S. degree from Purdue University, West Lafayette, IN, in 1996 and the M.S. and Ph.D. degrees from Vanderbilt University, Nashville, TN, in 1999 and 2001, respectively, all in mechanical engineering.

In 2001, she joined the Mechanical Engineering and Materials Science Department, Rice University, Houston, TX, where she is currently an Assistant Professor. Her current research interests include nanorobotic manipulation with haptic (force) feedback, haptic feedback and shared control between robotic devices and their human users for training and rehabilitation in virtual environments, control methodologies for improved performance of haptic interfaces and teleoperator systems, and educational haptics.

Dr. O'Malley is the 2004 ONR Young Investigator and the recipient of the NSF CAREER Award in 2005.